INFLUENCE OF DIFFERENT INTEGRAL KERNELS ON THE SOLUTIONS OF
BOUNDARY INTEGRAL EQUATIONS IN PLANE ELASTICITY

Y. Z. Chen, X. Y. Lin and Z. X. Wang

INFLUENCE OF DIFFERENT INTEGRAL KERNELS ON THE SOLUTIONS OF BOUNDARY INTEGRAL EQUATIONS IN PLANE ELASTICITY

Y. Z. CHEN, X. Y. LIN AND Z. X. WANG

A modified integral kernel is introduced for boundary integral equations (BIE). The formulation for the modified kernel is based on a representation in pure deformable form of the fundamental solution of concentrated forces. It is found that the modified kernel can be applied to any case, even if the loadings on the contour are not in equilibrium in an exterior boundary value problem. The influence of different integral kernels on solutions of BIE, particularly in the Neumann problem and Dirichlet problem, are addressed. Numerical examples are presented to prove the assertion proposed. Properties of solutions from the usage of the modified integral kernel are studied in detail. The influence of different integral kernels on the degenerate scale are discussed and numerical results are provided. It is found that the influence of the constants involved in the integral kernels is significant. For the cases of the elliptic and rectangular contour, the influence on the degenerate scale is studied with numerical results.

1. Introduction

The boundary integral equation (BIE) is widely used in elasticity. The fundamentals of BIE are found in [Rizzo 1967; Cruse 1969; Jaswon and Symm 1977; Brebbia et al. 1984]. Recent development of the boundary element method is summarized in [Cheng and Cheng 2005].

There are still some problems in the study of BIEs. The first is the regularity condition in the exterior boundary value problem (BVP) [Brebbia et al. 1984]. Generally, Betti's reciprocal theorem or the Somigliana identity is used for the formulation of the BIE. In the exterior BVP, if a mutual work difference integral (MWDI) on a sufficient large circle vanishes, the regularity condition is satisfied. However, this condition has not been studied clearly. Once the BIE in plane elasticity is formulated for the exterior region, one must meet the MWDI (the terms $D_{i(CR)}^{*1}(\xi)$ and $D_{i(CR)}^{*2}(\xi)$ in Equations (8) and (17)). If the MWDI vanishes, the regularity condition at infinity is satisfied. In fact, the MWDI is the difference of two works: the work done by the fundamental field on the physical stress field and vice versa. Therefore, the properties of the MWDI depend on the representation of the fundamental field and the properties of the physical stress field. A general expression for the MWDI from the two stress fields was obtained in [Chen 2003]. This will be the theoretical basis of the present study.

In fact, it has been proved that if the loadings applied on the contour in the exterior BVP are not in equilibrium, instead of using the usual integral kernel $U_{ij}^{*2}(\xi, x)$ (see (14)) one should use a modified one $U_{ij}^{*1}(\xi, x)$ (see (6)). The two integral kernels have a difference of a constant. Clearly, the two different integral kernels will influence the properties of solutions obtained.

The second problem in this field is the degenerate scale problem [He et al. 1996; Chen et al. 2002; 2005; Vodicka and Mantic 2008; Chen and Shen 2007]. In the degenerate scale problem, an improper solution in the Dirichlet problem for BIE exists if the used size is near the critical value. Clearly, the degenerate scale for the individual problem must depend on the used integral kernel, (for example, $U_{ij}^{*1}(\xi, x)$ or $U_{ij}^{*2}(\xi, x)$). This problem has also not been investigated in detail.

This paper complements the usual integral kernel $U_{ij}^{*2}(\xi, x)$ (see (14)) with a modified one, $U_{ij}^{*1}(\xi, x)$ (see (6)). The formulation for the modified kernel is based on a representation in pure deformable form of the fundamental solution of concentrated forces. The two kernels $U_{ij}^{*1}(\xi, x)$ and $U_{ij}^{*2}(\xi, x)$ have a difference of a constant. It is found that $U_{ij}^{*1}(\xi, x)$ can be used to any case, even if the loadings on the contour are not in equilibrium in an exterior BVP. The influence of the different integral kernels on solutions of the BIE, particularly in the Neumann problem and the Dirichlet problem, are addressed. The properties of solution using $U_{ij}^{*1}(\xi, x)$ are discussed in detail. Numerical examples are presented to prove the assertion proposed. The influence of the used integral kernels on the degenerate scale is discussed and numerical results are provided. It is found that the influence of the constant in the integral kernels on the degenerate scale is significant. For the cases of elliptic and rectangular contours, the influence is studied with numerical results.

2. Influence of different kernels on the solutions of exterior BIE

2.1. *Formulation of kernels $U_{ij}^{*1}(\xi, x)$ and $U_{ij}^{*2}(\xi, x)$ and the relevant BIEs.* The following analysis depends on the complex variable function method in plane elasticity [Muskhelishvili 1953]. In this method, the stresses $(\sigma_x, \sigma_y, \sigma_{xy})$, the resultant forces (X, Y), and the displacements (u, v) are expressed in terms of the two complex potentials $\phi(z)$ and $\psi(z)$ such that

$$\sigma_x + \sigma_y = 4 \operatorname{Re} \phi'(z), \quad \sigma_y - \sigma_x + 2i\sigma_{xy} = 2[\bar{z}\phi''(z) + \psi'(z)], \tag{1}$$

$$f = -Y + iX = \phi(z) + z\overline{\phi'(z)} + \overline{\psi(z)}, \tag{2}$$

$$2G(u + iv) = \kappa\phi(z) - z\overline{\phi'(z)} - \overline{\psi(z)}, \tag{3}$$

where $z = x + iy$ denotes a complex variable, G is the shear modulus of elasticity, $\kappa = (3 - v)/(1 + v)$ for the plane stress problems, $\kappa = 3 - 4v$ for the plane strain problems, and v is Poisson's ratio. In the present study, the plane strain condition is assumed throughout. In the following, we occasionally rewrite the displacements u and v as u_1 and u_2; σ_x, σ_y, and σ_{xy} as σ_{11}, σ_{22}, and σ_{12}; and x and y as x_1 and x_2, respectively.

It is emphasized that we only consider the exterior BVP. Also, the remote tractions σ_x^∞, σ_y^∞, and σ_{xy}^∞ are assumed to tend to zero.

The formulation of the BIE is introduced below. If the concentrated forces (P_x, P_y) are applied at the point $z = t$ (Figure 1a), the relevant complex potentials are defined by

$$\phi_{(\alpha)}(z) = F \ln(z - t), \quad \psi_{(\alpha)}(z) = -\kappa \bar{F} \ln(z - t) - \frac{F\bar{t}}{z - t} \tag{4}$$

(see [Muskhelishvili 1953]), where

$$F = -\frac{P_x + i P_y}{2\pi(\kappa + 1)}. \tag{5}$$

In (4), the subscript (α) denotes the fundamental solution initiated by concentrated forces.

Note that the relevant complex potentials shown in (4) are expressed in a pure deformable form [Chen and Lin 2008].

A direct substitution from the complex potentials shown in (4) in the proper place will lead to the following kernel [Chen and Lin 2008]:

$$U_{ij}^{*1}(\xi, x) = \frac{1}{8\pi(1-v)G}\left(-(3-4v)\ln(r)\delta_{ij} + r_{,i}r_{,j} - 0.5\delta_{ij}\right), \tag{6}$$

which is used in a BIE mentioned below.

Without losing generality, we can introduce the BIE for the region between the elliptic contour Γ and a large circle CR (Figure 1b). The observation point ξ is assumed on the elliptic contour $\xi \in \Gamma$. For the plane strain case, the suggested BIE can be written as follows [Brebbia et al. 1984]:

$$\tfrac{1}{2}u_i(\xi) + \int_\Gamma P_{ij}^*(\xi, x)u_j(x)\,ds(x) = \int_\Gamma U_{ij}^{*1}(\xi, x)p_j(x)\,ds(x) + D_{i(\text{CR})}^{*1}(\xi) \quad (i=1,2,\ \xi \in \Gamma), \tag{7}$$

where $D_{i(\text{CR})}^{*1}(\xi)$ is a MWDI on a large circle CR and is defined by

$$D_{i(\text{CR})}^{*1}(\xi) = -\int_{\text{CR}} P_{ij}^*(\xi, x)u_j(x)\,ds(x) + \int_{\text{CR}} U_{ij}^{*1}(\xi, x)p_j(x)\,ds(x) \quad (i=1,2,\ \xi \in \Gamma). \tag{8}$$

In (8), CR denotes the sufficient large circle with radius R.

In addition, the kernel $P_{ij}^*(\xi, x)$ is defined by [Brebbia et al. 1984]

$$P_{ij}^*(\xi, x) = -\frac{1}{4\pi(1-v)}\frac{1}{r}\left\{(r_{,1}n_1 + r_{,2}n_2)\left((1-2v)\delta_{ij} + 2r_{,i}r_{,j}\right) + (1-2v)(n_i r_{,j} - n_j r_{,i})\right\}, \tag{9}$$

where the Kronecker delta δ_{ij} is defined as $\delta_{ij} = 1$ for $i = j$, $\delta_{ij} = 0$ for $i \neq j$, and

$$r_{,1} = \frac{x_1 - \xi_1}{r} = \cos\alpha, \quad r_{,2} = \frac{x_2 - \xi_2}{r} = \sin\alpha, \qquad n_1 = -\sin\beta, \quad n_2 = \cos\beta, \tag{10}$$

where angles α and β are indicated in Figure 1.

Even the physical field is caused by a nonequilibrium force on the elliptic contour. We have proved in [Chen and Lin 2008] that $D_{i(\text{CR})}^{*1}(\xi) = 0$ $(i = 1, 2)$:

$$D_{i(\text{CR})}^{*1}(\xi) = -\int_{\text{CR}} P_{ij}^*(\xi, x)u_j(x)\,ds(x) + \int_{\text{CR}} U_{ij}^{*1}(\xi, x)p_j(x)\,ds(x) = 0 \quad (i=1,2,\ \xi \in \Gamma). \tag{11}$$

Therefore, (7) can be reduced to

$$\tfrac{1}{2}u_i(\xi) + \int_\Gamma P_{ij}^*(\xi, x)u_j(x)\,ds(x) = \int_\Gamma U_{ij}^{*1}(\xi, x)p_j(x)\,ds(x) \quad (i=1,2,\ \xi \in \Gamma). \tag{12}$$

Note that the displacements $u_j(x)$ on the left side of (12) should be expressed in pure deformable form.

In addition, if the same concentrated forces (P_x, P_y) are applied at the point $z = t$ (Figure 1a), the relevant complex potentials can be defined alternatively by [Muskhelishvili 1953]

$$\phi_{(\alpha)}(z) = F\ln(z-t), \qquad \psi_{(\alpha)}(z) = -\kappa\bar{F}\ln(z-t) - \frac{F\bar{t}}{z-t} + \bar{F}. \tag{13}$$

The complex potentials shown in (13) differ from those in (4) by a constant $\bar{F}$ in the function $\psi_{(\alpha)}(z)$.

Comparing (4) with (13), an additional pair of complex potentials $\phi(z) = 0$ and $\psi(z) = \bar{F}$ is presented in (13). Clearly, this pair causes no stresses anywhere, and represents a rigid translation. Therefore, it is said that the complex potentials in (13) are expressed in an impure deformable form.

A direct substitution from the complex potentials in (13) in the proper place will lead to the following kernel [Chen and Lin 2008]:

$$U_{ij}^{*2}(\xi, x) = \frac{1}{8\pi(1-\nu)G}\left(-(3-4\nu)\ln(r)\delta_{ij} + r_{,i}r_{,j}\right). \tag{14}$$

The two kernels have the relation

$$U_{ij}^{*2}(\xi, x) - U_{ij}^{*1}(\xi, x) = \frac{1}{16\pi(1-\nu)G}\delta_{ij}. \tag{15}$$

The kernel $U_{ij}^{*2}(\xi, x)$ is found in [Brebbia et al. 1984]. Similarly, from the kernel $U_{ij}^{*2}(\xi, x)$ in (14), we obtain the BIE

$$\tfrac{1}{2}u_i(\xi) + \int_\Gamma P_{ij}^*(\xi, x)u_j(x)\,ds(x) = \int_\Gamma U_{ij}^{*2}(\xi, x)p_j(x)\,ds(x) + D_{i(CR)}^{*2}(\xi) \quad (i = 1, 2, \ \xi \in \Gamma), \tag{16}$$

where $D_{i(CR)}^{*2}(\xi)$ is a MWDI on a large circle and is defined by

$$D_{i(CR)}^{*2}(\xi) = -\int_{CR} P_{ij}^*(\xi, x)u_j(x)\,ds(x) + \int_{CR} U_{ij}^{*2}(\xi, x)p_j(x)\,ds(x) \quad (i = 1, 2, \ \xi \in \Gamma). \tag{17}$$

It was proved in [Chen and Lin 2008] that when the physical field is caused by a nonequilibrium force on the elliptic contour, we have $D_{i(CR)}^{*2}(\xi) \neq 0$ for $i = 1, 2$ (so the BIE (16) cannot be reduced further), while in the opposite case — when the physical field is caused by an equilibrium force on the elliptic contour — we have $D_{i(CR)}^{*2}(\xi) = 0$ for $i = 1, 2$, and then the BIE (16) can be reduced to the form

$$\tfrac{1}{2}u_i(\xi) + \int_\Gamma P_{ij}^*(\xi, x)u_j(x)\,ds(x) = \int_\Gamma U_{ij}^{*2}(\xi, x)p_j(x)\,ds(x) \quad (i = 1, 2, \ \xi \in \Gamma). \tag{18}$$

Note that in the exterior BVP, the BIE using the kernel $U_{ij}^{*1}(\xi, x)$, shown by (6), can always be used, even if the applied loadings on the elliptic contour are not in equilibrium. However, in the exterior BVP, the BIE using $U_{ij}^{*2}(\xi, x)$, shown by (14), can only be used when the applied loadings on the elliptic contour are in equilibrium.

2.2. General properties of the solutions of BIEs. As claimed previously, the kernel $U_{ij}^{*1}(\xi, x)$ can always be used, without regard to the loading condition on the elliptic contour. Therefore, for the exterior BVP we suggest the BIE (12), which we repeat here for convenience:

$$\tfrac{1}{2}u_i(\xi) + \int_\Gamma P_{ij}^*(\xi, x)u_j(x)\,ds(x) = \int_\Gamma U_{ij}^{*1}(\xi, x)p_j(x)\,ds(x) \quad (i = 1, 2, \ \xi \in \Gamma). \tag{19}$$

The problem of the equivalence of the solution of the BIE and an elasticity solution is studied below. As stated previously, the physical stress field is assumed in pure deformable form. Therefore, if the functions $u_i(\xi)$, $u_j(x)$, and $p_j(x)$ in (12) are boundary values of an elasticity solution expressed in pure deformable form, these functions must satisfy the BIE in (12); if $u_i(\xi)$, $u_j(x)$, and $p_j(x)$ in (12) are
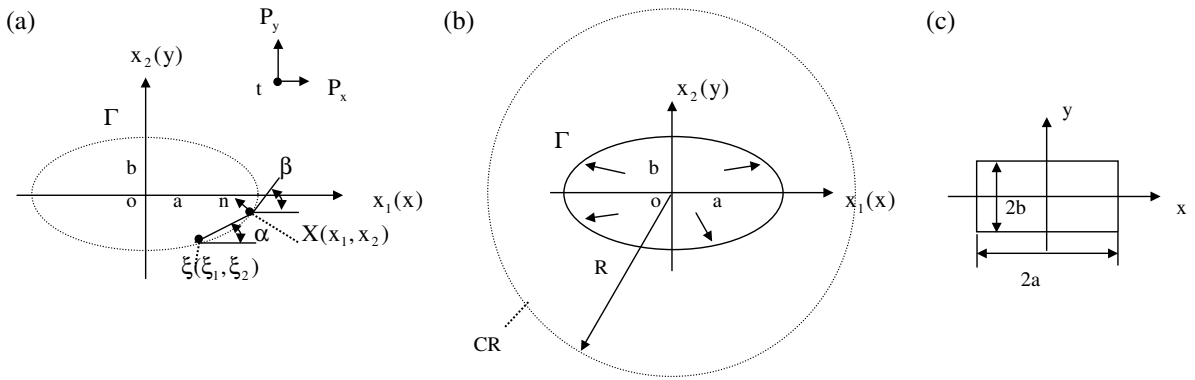
Figure 1. (a) A concentrated force applied at point $z = t$, or the loading condition for the α-field. (b) Some loadings having resultant forces applied on the elliptic contour, or the loading condition for the β-field or physical stress field. (c) A rectangular notch.

boundary values of an elasticity solution expressed in an impure deformable form, they must not satisfy the BIE shown by (12).

This situation can be seen from the following example. It is known that there are three particular elasticity solutions:

$$
\begin{Bmatrix} u_1^{(1)} \\ u_2^{(1)} \end{Bmatrix} = \begin{Bmatrix} b_1^{(1)} \\ b_2^{(1)} \end{Bmatrix} = \begin{Bmatrix} 1 \\ 0 \end{Bmatrix}, \qquad \sigma_{ij}^{(1)} = 0 \text{ and } p_i^{(1)} = 0,
$$

$$
\begin{Bmatrix} u_1^{(2)} \\ u_2^{(2)} \end{Bmatrix} = \begin{Bmatrix} b_1^{(2)} \\ b_2^{(2)} \end{Bmatrix} = \begin{Bmatrix} 0 \\ 1 \end{Bmatrix}, \qquad \sigma_{ij}^{(2)} = 0 \text{ and } p_i^{(2)} = 0, \tag{20}
$$

$$
\begin{Bmatrix} u_1^{(3)} \\ u_2^{(3)} \end{Bmatrix} = \begin{Bmatrix} b_1^{(3)} \\ b_2^{(3)} \end{Bmatrix} = \begin{Bmatrix} -y_t \\ x_t \end{Bmatrix}, \qquad \sigma_{ij}^{(3)} = 0 \text{ and } p_i^{(3)} = 0 \quad (t = x_t + iy_t \in \Gamma).
$$

Clearly, the stress fields shown by (20) represent translations or rotation for the body. It has been proved that substituting those displacements on the contour into the left-hand term of (12) yields

$$
\frac{1}{2} u_i(\xi) + \int_\Gamma P_{ij}^*(\xi, x) u_j(x) \, ds(x) \Bigg|_{u_i \to b_i^{(k)}} = b_i^{(k)} \neq 0 \quad (k = 1, 2, 3). \tag{21}
$$

Substituting the tractions $p_j(x)$ on the contour shown by (20) into right-hand term of (12) yields

$$
\int_\Gamma U_{ij}^{*1}(\xi, x) p_j(x) \, ds(x) \Bigg|_{p_j \to p_j^{(k)} = 0} = 0. \tag{22}
$$

Comparing (21) and (22), which are the left and right sides of (12) respectively, proves the assertion.

In the Neumann problem, the boundary tractions $\tilde{p}_j(x)$ ($j = 1, 2$) are given beforehand. Therefore, in the case of the kernel $U_{ij}^{*1}(\xi, x)$, from (12) we can obtain the BIE

$$
\frac{1}{2} u_i(\xi) + \int_\Gamma P_{ij}^*(\xi, x) u_j(x) \, ds(x) = g_i(\xi) \quad (i = 1, 2, \ \xi \in \Gamma), \tag{23}
$$

where

$$g_i(\xi) = \int_\Gamma U_{ij}^{*1}(\xi, x)\tilde{p}_j(x)\,ds(x) \quad (i = 1, 2, \ \xi \in \Gamma). \tag{24}$$

In (24), $\tilde{p}_j(x)$ ($j = 1, 2$) are the boundary tractions which are given beforehand.

It is known that the BIE in (23) possesses the invertible property; that is, it can be solved for any right-hand term $g_i(\xi)$. However, the obtained $u_j(x)$ ($j = 1, 2$) belong to some boundary values of displacements in an elasticity solution expressed in pure deformable form.

Similarly, in the Dirichlet problem, the boundary displacements $\tilde{u}_j(x)$ ($j = 1, 2$) are given beforehand. Therefore, in the case of the kernel $U_{ij}^{*1}(\xi, x)$, from (12) we can obtain the BIE

$$\int_\Gamma U_{ij}^{*1}(\xi, x)p_j(x)\,ds(x) = h_i(\xi) \quad (i = 1, 2, \ \xi \in \Gamma), \tag{25}$$

where

$$h_i(\xi) = \tfrac{1}{2}\tilde{u}_i(\xi) + \int_\Gamma P_{ij}^*(\xi, x)\tilde{u}_j(x)\,ds(x) \quad (i = 1, 2, \ \xi \in \Gamma). \tag{26}$$

In (26), $\tilde{u}_i(\xi)$ ($i = 1, 2$) and $\tilde{u}_j(x)$ ($j = 1, 2$) are the boundary displacements, which are given beforehand.

It is known that the BIE shown by (25) processes the invertible property only if the degenerate scale has not been reached [Vodicka and Mantic 2008]. In other words, the BIE shown by (25) can be solved for any right-hand term $h_i(\xi)$ only if the degenerate scale has not been reached. However, the obtained $p_j(x)$ ($j = 1, 2$) belong to some boundary values of tractions in an elasticity solution. Generally, those tractions, $p_j(x)$ ($j = 1, 2$), may have a resultant force along the contour.

2.3. Numerical investigation of the kernels $U_{ij}^{*1}(\xi, x)$ and $U_{ij}^{*2}(\xi, x)$ in the case of nonequilibrium loadings on the contour.
In order to examine the behavior of the kernels $U_{ij}^{*1}(\xi, x)$ and $U_{ij}^{*2}(\xi, x)$, the relevant BIEs are repeated:

$$\tfrac{1}{2}u_i(\xi) + \int_\Gamma P_{ij}^*(\xi, x)u_j(x)\,ds(x) = \int_\Gamma U_{ij}^{*1}(\xi, x)p_j(x)\,ds(x) \quad (i = 1, 2, \ \xi \in \Gamma), \tag{27}$$

$$\tfrac{1}{2}u_i(\xi) + \int_\Gamma P_{ij}^*(\xi, x)u_j(x)\,ds(x) = \int_\Gamma U_{ij}^{*2}(\xi, x)p_j(x)\,ds(x) \quad (i = 1, 2, \ \xi \in \Gamma). \tag{28}$$

In all the problems studied subsequently, one knows a closed-form solution beforehand. Substituting the results from the known solution, say for $p_j(x)$ ($j = 1, 2$), into the right-hand term of (12) will yield a BIE for $u_j(x)$ ($j = 1, 2$). The displacements $u_j(x)$ ($j = 1, 2$) can be obtained from the BIE, and then compared with those from the closed-form solution. In the solution of the BIE, the scale used is assumed to be sufficient large to avoid the used scale coinciding with the degenerate scale.

In the examples below, the ellipse has major semiaxis a and minor semiaxis b (Figure 1b). The plane strain condition and $\nu = 0.3$ are assumed. The elliptic contour is divided into 120 intervals. For the BIE solution, constant displacement and traction are assumed for each interval.

Example 1. We propose the complex potentials

$$\phi(z) = q_0 A \ln z, \quad \psi(z) = -\kappa q_0 \bar{A} \ln z, \quad \text{where } A = A_1 + i A_2, \tag{29}$$

where q_0 is a unit loading. From the complex potentials shown by (29) and (2), it can be seen that the following resultant forces are applied:

$$\{X + iY\}_{\text{re}} = -2\pi(\kappa + 1)q_0 A, \tag{30}$$

on the contour. In this case, the exact solution for the displacements and stresses on the boundary contour can be easily obtained from (1), (3) and (29).

In this example, the examination is performed from the viewpoint of the Neumann problem. The loadings applied on the contour, p_j ($j = 1, 2$), are computed from the complex potentials in (29), and are then substituted into the right-hand term of (18). Standard numerical techniques are used to solve (18), and the boundary displacements u_j ($j = 1, 2$) can be evaluated immediately. The calculated boundary displacements using the kernels $U_{ij}^{*1}(\xi, x)$ and $U_{ij}^{*2}(\xi, x)$, and those from the exact solution are expressed by

$$u_1 = \frac{q_0}{2G(1+v)} f_1(\theta), \qquad u_2 = \frac{q_0}{2G(1+v)} f_2(\theta), \qquad \text{(at the points } x = a\cos\theta, \ y = b\cos\theta). \tag{31}$$

For the case of $b/a = 0.25$, $a = 40$, $A_1 = 1$, and $A_2 = 0.5$, the results calculated using the kernels $U_{ij}^{*1}(\xi, x)$ and $U_{ij}^{*2}(\xi, x)$, and the exact results from the closed-form solution are shown in Figure 2, where $f_1(\theta)_{\text{ex}}$ and $f_2(\theta)_{\text{ex}}$ are from the exact solution, or from the complex potentials (29) directly; $f_1(\theta)_{*1}$ and $f_2(\theta)_{*1}$ are from the usage of the kernels $U_{ij}^{*1}(\xi, x)$; and $f_1(\theta)_{*2}$ and $f_2(\theta)_{*2}$ are from the usage of the kernels $U_{ij}^{*2}(\xi, x)$.

It is found from Figure 2 that the results computed for $f_1(\theta)_{*1}$ and $f_2(\theta)_{*1}$ using the kernel $U_{ij}^{*1}(\xi, x)$ are very accurate, coinciding with the results from the exact solution (denoted by $f_1(\theta)_{\text{ex}}$ and $f_2(\theta)_{\text{ex}}$). However, the results computed for $f_1(\theta)_{*2}$ and $f_2(\theta)_{*2}$ using the kernel $U_{ij}^{*2}(\xi, x)$ are very different from
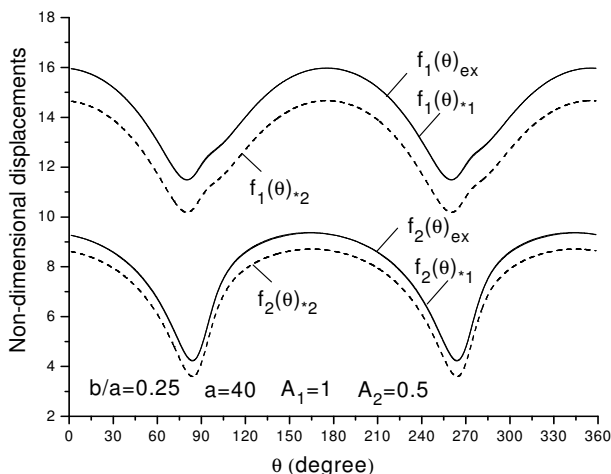

Figure 2. Nondimensional displacements for an exterior problem with nonequilibrium loadings on contour: $f_1(\theta)_{\text{ex}}$ and $f_2(\theta)_{\text{ex}}$ from the exact solution, $f_1(\theta)_{*1}$ and $f_2(\theta)_{*1}$ from the kernel $U_{ij}^{*1}(\xi, x)$, from $f_1(\theta)_{*2}$ and $f_2(\theta)_{*2}$ using $U_{ij}^{*2}(\xi, x)$, with $b/a = 0.25$, $a = 40$, $A_1 = 1$, and $A_2 = 0.5$ in (29) (see Figure 1b and (31)).
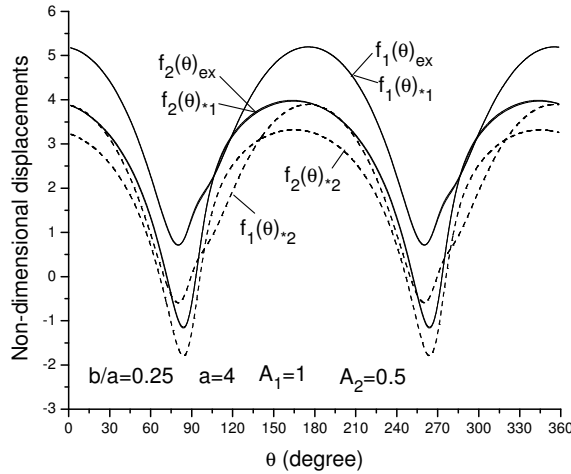
Figure 3. Nondimensional displacements for an exterior problem with nonequilibrium loadings on contour: $f_1(\theta)_{ex}$ and $f_2(\theta)_{ex}$ from the exact solution, $f_1(\theta)_{*1}$ and $f_2(\theta)_{*1}$ from the kernel $U_{ij}^{*1}(\xi, x)$, and $f_1(\theta)_{*2}$ and $f_2(\theta)_{*2}$ from $U_{ij}^{*2}(\xi, x)$, with $b/a = 0.25$, $a = 4$, $A_1 = 1$, and $A_2 = 0.5$ in (29) (see Figure 1b and (31)).

those from the exact solution. It is also found that the results computed for $f_1(\theta)_{*2}$ and $f_2(\theta)_{*2}$ have a constant difference from $f_1(\theta)_{ex}$ and $f_2(\theta)_{ex}$.

Similarly, in the case of $b/a = 0.25$, $a = 4$, $A_1 = 1$, and $A_2 = 0.5$, the results calculated using the kernels $U_{ij}^{*1}(\xi, x)$ and $U_{ij}^{*2}(\xi, x)$ and the exact results from the closed-form solution are shown in Figure 3. Similar phenomena as in the previous case can be observed.

Example 2. All the conditions used in Example 1 are still used in this example. However, in this example, the examination is performed from the viewpoint of the Dirichlet problem. The displacements on the contour, u_j ($j = 1, 2$), are computed from the complex potentials shown by (29), and the obtained displacements u_j ($j = 1, 2$) are substituted into the left-hand term of (12) (or (18)). Standard numerical technique is used to solve (12) (or (18)), and the boundary tractions p_j ($j = 1, 2$) can be evaluated immediately. The calculated boundary tractions are expressed by

$$p_1 = q_0 g_1(\theta), \quad p_2 = q_0 g_2(\theta) \qquad \text{(at the points } x = a\cos\theta,\ x = b\cos\theta\text{)}. \tag{32}$$

For the case of $b/a = 0.25$, $a = 40$, $A_1 = 1$, and $A_2 = 0.5$, the results calculated using the kernels $U_{ij}^{*1}(\xi, x)$ and $U_{ij}^{*2}(\xi, x)$, and the exact results from the closed-form solution are shown in Figure 4, where $g_1(\theta)_{ex}$ and $g_2(\theta)_{ex}$ are from exact solution, or from the complex potentials (29) directly, $g_1(\theta)_{*1}$ and $g_2(\theta)_{*1}$ are from the usage of the kernels $U_{ij}^{*1}(\xi, x)$, and $g_1(\theta)_{*2}$ and $g_2(\theta)_{*2}$ are from the usage the kernels $U_{ij}^{*2}(\xi, x)$.

It is found from Figure 4 that the results computed for $g_1(\theta)_{*1}$ and $g_2(\theta)_{*1}$ using the kernel $U_{ij}^{*1}(\xi, x)$ are very accurate, which coincides with the results from the exact solution (denoted by $g_1(\theta)_{ex}$ and $g_2(\theta)_{ex}$). However, the results computed for $g_1(\theta)_{*2}$ and $g_2(\theta)_{*2}$ using the kernel $U_{ij}^{*2}(\xi, x)$ are very different from those from the exact solution (denoted by $g_1(\theta)_{ex}$ and $g_2(\theta)_{ex}$).
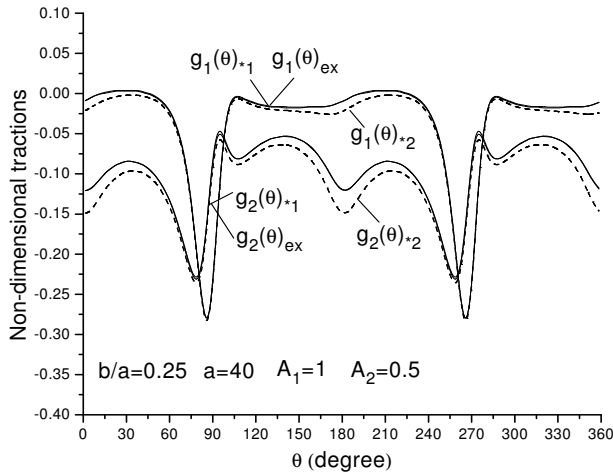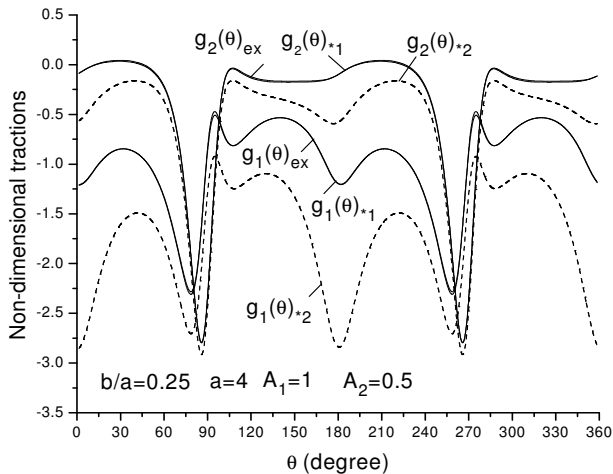
Figure 4. Nondimensional tractions for an exterior problem with nonequilibrium loadings on contour: $g_1(\theta)_{ex}$ and $g_2(\theta)_{ex}$ from the exact solution, $g_1(\theta)_{*1}$ and $g_2(\theta)_{*1}$ from the kernel $U_{ij}^{*1}(\xi, x)$, and $g_1(\theta)_{*2}$ and $g_2(\theta)_{*2}$ from $U_{ij}^{*2}(\xi, x)$, with $b/a = 0.25$, $a = 40$, $A_1 = 1$, and $A_2 = 0.5$ in (29) (see Figure 1b and (32)).

Similarly, in the case of $b/a = 0.25$, $a = 4$, $A_1 = 1$, and $A_2 = 0.5$, the results calculated using the kernels $U_{ij}^{*1}(\xi, x)$ and $U_{ij}^{*2}(\xi, x)$ and the exact results from the closed-form solution are shown in Figure 5. Similar results as in the previous case have been found. Particularly, in this case, the deviation of the result using the kernel $U_{ij}^{*2}(\xi, x)$ can reach a higher value. For example, in the case of $\theta = \pi$ we have $g_1(\theta)_{ex} = -1.195$ from the exact solution, $g_1(\theta)_{*1} = -1.200$ using the kernel $U_{ij}^{*1}(\xi, x)$, and $g_1(\theta)_{*2} = -2.842$ using the kernel $U_{ij}^{*2}(\xi, x)$; see Figure 5.

Figure 5. Nondimensional tractions for an exterior problem with nonequilibrium loadings on contour: $g_1(\theta)_{ex}$ and $g_2(\theta)_{ex}$ from the exact solution, $g_1(\theta)_{*1}$ and $g_2(\theta)_{*1}$ from the kernel $U_{ij}^{*1}(\xi, x)$, and $g_1(\theta)_{*2}$ and $g_2(\theta)_{*2}$ from $U_{ij}^{*2}(\xi, x)$, with $b/a = 0.25$, $a = 4$, $A_1 = 1$, and $A_2 = 0.5$ in (29) (see Figure 1b and (32)).

2.4. *Numerical investigation of the kernels $U_{ij}^{*1}(\xi, x)$ and $U_{ij}^{*2}(\xi, x)$ in the case of equilibrium loadings on the contour.* As mentioned previously, in the case of equilibrium loadings on the contour, the solutions obtained from the two kinds of BIE shown in (12) and (18) must be the same. This conclusion is also examined in the following examples.

Example 3. In this example, we propose the complex potentials

$$\phi(z) = q_0 \frac{A}{z}, \quad \psi(z) = q_0 \frac{B}{z}, \quad \text{where } A = A_1 + i A_2, \quad B = B_1 + i B_2, \tag{33}$$

where q_0 is a unit loading. From the complex potentials in (33) we see that the loadings applied on the contour must be in equilibrium [Muskhelishvili 1953].

Similarly, in the Neumann problem, the calculated boundary displacements using the kernel $U_{ij}^{*1}(\xi, x)$ or $U_{ij}^{*2}(\xi, x)$ and those from the exact solution are expressed by

$$u_1 = \frac{q_0}{2G(1+v)} f_1(\theta), \quad u_2 = \frac{q_0}{2G(1+v)} f_2(\theta) \quad (\text{at the points } x = a \cos\theta, \ x = b \cos\theta). \tag{34}$$

For the case of $b/a = 0.25$, $a = 40$, $A_1 = 1$, $A_2 = 0.5$, $B_1 = 1$, and $B_2 = 0.5$ the calculated results using the kernels $U_{ij}^{*1}(\xi, x)$ and $U_{ij}^{*2}(\xi, x)$ and the exact results from the closed-form solution are shown in Figure 6, where $f_1(\theta)_{ex}$ and $f_2(\theta)_{ex}$ are from exact solution, or from the complex potentials (33) directly; $f_1(\theta)_{*1}$ and $f_2(\theta)_{*1}$ are from the usage of the kernels $U_{ij}^{*1}(\xi, x)$, while $f_1(\theta)_{*2}$ and $f_2(\theta)_{*2}$ are from the usage of $U_{ij}^{*2}(\xi, x)$.

It is found from Figure 6 that the results computed using the kernel $U_{ij}^{*1}(\xi, x)$ or $U_{ij}^{*2}(\xi, x)$ and those from the exact solution are merged into the same curves.

Example 4. All the conditions used in Example 3 are still used in this example. However, in this example, the examination is performed from the viewpoint of the Dirichlet problem. The displacements on the
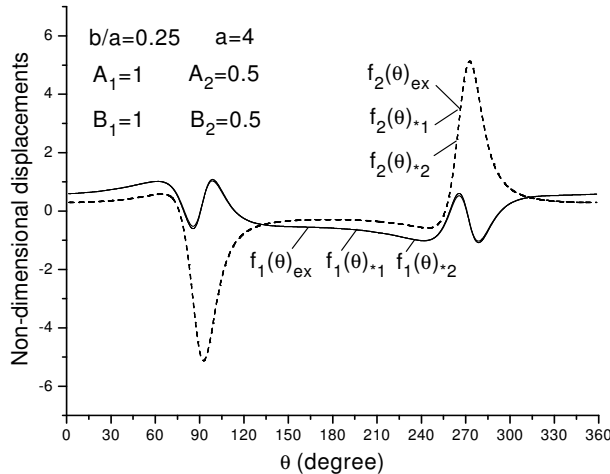

Figure 6. Nondimensional displacements for an exterior problem with nonequilibrium loadings on contour: $f_1(\theta)_{ex}$ and $f_2(\theta)_{ex}$ from the exact solution, $f_1(\theta)_{*1}$ and $f_2(\theta)_{*1}$ from the kernel $U_{ij}^{*1}(\xi, x)$, and $f_1(\theta)_{*2}$, and $f_2(\theta)_{*2}$ from $U_{ij}^{*2}(\xi, x)$, with $b/a = 0.25$, $a = 4$, $A_1 = 1$, $A_2 = 0.5$, $B_1 = 1$, and $B_2 = 0.5$ in (33) (see Figure 1b and (31)).
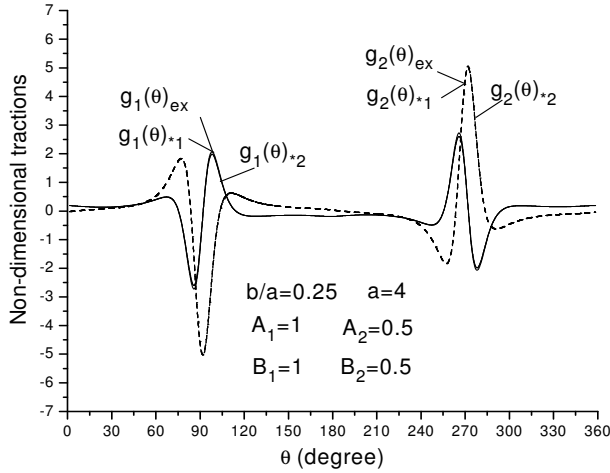
Figure 7. Nondimensional tractions for an exterior problem with nonequilibrium load-ings on contour: $g_1(\theta)_{\text{ex}}$ and $g_2(\theta)_{\text{ex}}$ from the exact solution, $g_1(\theta)_{*1}$ and $g_2(\theta)_{*1}$ from the kernel $U_{ij}^{*1}(\xi, x)$, and $g_1(\theta)_{*2}$, and $g_2(\theta)_{*2}$ from $U_{ij}^{*2}(\xi, x)$, with $b/a = 0.25$, $a = 4$, $A_1 = 1$, $A_2 = 0.5$, $B_1 = 1$, and $B_2 = 0.5$ in (33) (see Figure 1b and (32)).

contour, u_j $(j = 1, 2)$, are computed from the complex potentials in (33), and the obtained displacements u_j $(j = 1, 2)$ are substituted into the left-hand term of (12) (or (18)). The calculated boundary tractions are expressed by

$$p_1 = q_0 g_1(\theta), \quad p_2 = q_0 g_2(\theta) \quad \text{(at the points } x = a\cos\theta, \ x = b\cos\theta). \tag{35}$$

For the case of $b/a = 0.25$, $a = 40$, $A_1 = 1$, $A_2 = 0.5$, $B_1 = 1$, and $B_2 = 0.5$ the results calculated using the kernels $U_{ij}^{*1}(\xi, x)$ and $U_{ij}^{*2}(\xi, x)$ and the exact results from the closed-form solution are shown in Figure 7, where $g_1(\theta)_{\text{ex}}$ and $g_2(\theta)_{\text{ex}}$ are from exact solution, or from the complex potentials (33) directly; $g_1(\theta)_{*1}$ and $g_2(\theta)_{*1}$ are from the usage of the kernels $U_{ij}^{*1}(\xi, x)$, while $g_1(\theta)_{*2}$ and $g_2(\theta)_{*2}$ are from the usage of $U_{ij}^{*2}(\xi, x)$.

It is found from Figure 7 that the results computed from the usage of kernel $U_{ij}^{*1}(\xi, x)$ or $U_{ij}^{*2}(\xi, x)$ and those from the exact solution are merged into the same curves.

3. Numerical evaluations for degenerate scale problems for different kernels $U_{ij}^{*g}(\xi, x)$

Instead of the two kernels $U_{ij}^{*1}(\xi, x)$ and $U_{ij}^{*2}(\xi, x)$, a kernel $U_{ij}^{*g}(\xi, x)$ in a more general form is defined as

$$U_{ij}^{*g}(\xi, x) = \frac{1}{8\pi(1-\nu)G}\left(-(3-4\nu)\ln(r)\delta_{ij} + r_{,i}r_{,j} - s\delta_{ij}\right), \tag{36}$$

where s can take any real value.

Clearly, a homogeneous equation for the degenerate scale problem using the kernel $U_{ij}^{*g}(\xi, x)$ can be formulated:

$$\int_{\Gamma_d} U_{ij}^{*g}(\xi, x)p_j(x)\,ds(x) = 0 \quad (i = 1, 2, \xi \in \Gamma). \tag{37}$$

In the formulation, one wants to find a particular size such that (37) has a nontrivial solution for $p_j(x)$, or $p_j(x) \neq 0$. By using relevant solutions in the normal scale problem, the degenerate scale problem can be solved [Chen et al. 2005; Vodicka and Mantic 2008].

In [Chen et al. 2009], after using two fundamental solutions in the normal scale, the degenerate scale problem can be solved. In this paper, the method suggested in [Chen et al. 2009] is used to solve the problems in the next two examples. Clearly, the degenerate scale must depend on the assumed constant s in (36).

Example 5. In the example, the ellipse has major semiaxis a and minor semiaxis b (Figure 1b). In computation, the plane strain condition and $v = 0.3$ are assumed. The elliptic contour is divided into 120 intervals. For the BIE solution, the constant displacement and traction are assumed for each interval. We vary s from -0.5 to 1.5 in steps of 0.5, and b/a from 0.1 to 1.0 in steps of 0.1, and list in Table 1 the two degenerate scales

$$a_{d1} = f_1(s, b/a), \quad a_{d2} = f_2(s, b/a). \tag{38}$$

We see that as the value of s increases from -0.5 to 1.5, the degenerate scale becomes smaller and smaller.

Example 6. In the example, the rectangular notch has width $2a$ and height $2b$ (Figure 1c). For the same ranges of s and b/a as in the previous example, we list in Table 2 the two degenerate scales

$$a_{d1} = g_1(s, b/a), \quad a_{d2} = g_2(s, b/a). \tag{39}$$

Again, as s increases from -0.5 to 1.5, the degenerate scale becomes smaller and smaller.

$a_{d1} = f_1(s, b/a)$										
$b/a =$	0.1	0.2	0.3	0.4	0.5	0.6	0.7	0.8	0.9	1.0
s										
-0.5	2.52541	2.41447	2.30954	2.21105	2.11897	2.03305	1.95295	1.87824	1.80853	1.74340
0	1.91291	1.82888	1.74940	1.67479	1.60504	1.53997	1.47929	1.42270	1.36990	1.32057
0.5	1.44896	1.38531	1.32511	1.26860	1.21577	1.16647	1.12051	1.07765	1.03765	1.00028
1	1.09754	1.04932	1.00372	0.96092	0.92090	0.88356	0.84875	0.81628	0.78598	0.75768
1.5	0.83135	0.79483	0.76029	0.72786	0.69755	0.66927	0.64290	0.61830	0.59535	0.57392
$a_{d2} = f_2(s, b/a)$										
$b/a =$	0.1	0.2	0.3	0.4	0.5	0.6	0.7	0.8	0.9	1.0
s										
-0.5	3.97868	3.49681	3.11489	2.80545	2.55005	2.33597	2.15411	1.99784	1.86219	1.74340
0	3.01371	2.64871	2.35942	2.12503	1.93158	1.76942	1.63166	1.51329	1.41054	1.32057
0.5	2.28278	2.00631	1.78718	1.60963	1.46310	1.34027	1.23593	1.14627	1.06844	1.00028
1	1.72913	1.51971	1.35373	1.21924	1.10825	1.01521	0.93617	0.86826	0.80930	0.75768
1.5	1.30975	1.15112	1.02540	0.92353	0.83946	0.76899	0.70912	0.65767	0.61302	0.57392

Table 1. The degenerate scale $a_{d1} = f_1(s, b/a)$ and $a_{d2} = f_2(s, b/a)$ for an ellipse notch (see (38) and Figure 1b).

$a_{d1} = g_1(s, b/a)$

$b/a =$	0.1	0.2	0.3	0.4	0.5	0.6	0.7	0.8	0.9	1.0
s										
-0.5	2.40472	2.22301	2.07631	1.95320	1.84796	1.75521	1.67343	1.60015	1.53398	1.47394
0	1.82149	1.68385	1.57273	1.47948	1.39977	1.32951	1.26756	1.21206	1.16194	1.11646
0.5	1.37971	1.27546	1.19129	1.12066	1.06028	1.00706	0.96014	0.91809	0.88013	0.84568
1	1.04508	0.96612	0.90236	0.84886	0.80312	0.76281	0.72727	0.69542	0.66666	0.64057
1.5	0.79162	0.73180	0.68351	0.64298	0.60834	0.57780	0.55088	0.52676	0.50498	0.48521

$a_{d2} = g_2(s, b/a)$

$b/a =$	0.1	0.2	0.3	0.4	0.5	0.6	0.7	0.8	0.9	1.0
s										
-0.5	3.61122	3.04801	2.66064	2.37149	2.14534	1.96172	1.80951	1.68074	1.57017	1.47394
0	2.73537	2.30876	2.01534	1.79632	1.62502	1.48593	1.37064	1.27310	1.18935	1.11646
0.5	2.07195	1.74881	1.52655	1.36065	1.23090	1.12554	1.03821	0.96433	0.90089	0.84568
1	1.56943	1.32466	1.15631	1.03065	0.93236	0.85256	0.78641	0.73045	0.68239	0.64057
1.5	1.18879	1.00338	0.87587	0.78068	0.70623	0.64578	0.59568	0.55329	0.51689	0.48521

Table 2. The degenerate scale $a_{d1} = g_1(d, b/a)$ and $a_{d2} = g_2(d, b/a)$ for a rectangular notch (see (39) and Figure 1c).

4. Conclusions

From the our theoretical analysis and numerical examples we get the following conclusions. The kernel $U_{ij}^{*1}(\xi, x)$ can be used for arbitrary loading on the contour. However, the kernel $U_{ij}^{*2}(\xi, x)$ can only be used when the loading on the contour is in equilibrium. This is an effective way to examine a suggested boundary integral equation (BIE) by using a known solution, particularly through a solution expressed in complex potentials. In this case, since the solution is known beforehand, one can easily judge whether the formulation used in the computation is correct or not.

In the case of using the kernel $U_{ij}^{*1}(\xi, x)$, the properties of solutions of the BIE are clearly studied. If the degenerate scale has not been reached, the Dirichlet problem has a unique solution. Generally, the computed tractions on the boundary may result in resultant forces along the contour. In the Neumann problem, the computed displacements must belong to the boundary values of the displacement field expressed in pure deformable form.

In the degenerate scale problem, the constant s involved in the integral kernel $U_{ij}^{*g}(\xi, x)$ has a significant influence to the final results of the degenerate scale.

References

[Brebbia et al. 1984] C. A. Brebbia, J. C. F. Telles, and L. C. Wrobel, *Boundary element techniques – theory and applications in engineering*, Springer, Heidelberg, 1984.

[Chen 2003] Y. Z. Chen, "Analysis of L-integral and theory of the derivative stress field in plane elasticity", *Int. J. Solids Struct.* **40** (2003), 3589–3602.

[Chen and Lin 2008] Y. Z. Chen and X. Y. Lin, "Regularity condition and numerical examination for degenerate scale problem of BIE for exterior problem of plane elasticity", *Eng. Anal. Bound. Elem.* **32** (2008), 811–823.

[Chen and Shen 2007] J. T. Chen and W. C. Shen, "Degenerate scale for multiply connected Laplace problems", *Mech. Res. Commun.* **34** (2007), 69–77.

[Chen et al. 2002] J. T. Chen, S. R. Kuo, and J. H. Lin, "Analytical study and numerical experiments for degenerate scale problems in the boundary element method of two-dimensional elasticity", *Int. J. Numer. Meth. Eng.* **54** (2002), 1669–1681.

[Chen et al. 2005] J. T. Chen, S. R. Lin, and K. H. Chen, "Degenerate Scale problem when solving Laplace's equation by BEM and its treatment", *Int. J. Numer. Meth. Eng.* **62** (2005), 233–261.

[Chen et al. 2009] Y. Z. Chen, X. Y. Lin, and Z. X. Wang, "Numerical solution for degenerate scale problem for exterior multiply connected region", *Eng. Anal. Bound. Elem.* **33** (2009), 1316–1321.

[Cheng and Cheng 2005] A. H. D. Cheng and D. S. Cheng, "Heritage and early history of the boundary element method", *Eng. Anal. Bound. Elem.* **29** (2005), 286–302.

[Cruse 1969] T. A. Cruse, "Numerical solutions in three-dimensional elastostatics", *Int. J. Solids Struct.* **5** (1969), 1259–1274.

[He et al. 1996] W. J. He, H. J. Ding, and H. C. Hu, "Degenerate scale and boundary element analysis of two dimensional potential and elasticity problems", *Comput. Struct.* **60** (1996), 155–158.

[Jaswon and Symm 1977] M. A. Jaswon and G. T. Symm, *Integral equation methods in potential theory and elastostatics*, Academic Press, London, 1977.

[Muskhelishvili 1953] N. I. Muskhelishvili, *Some basic problems of mathematical theory of elasticity*, Noordhoof, Amsterdam, 1953.

[Rizzo 1967] F. J. Rizzo, "An integral equation approach to boundary value problems in classical elastostatics", *Quart. J. Appl. Math.* **25** (1967), 83–95.

[Vodicka and Mantic 2008] R. Vodicka and V. Mantic, "On solvability of a boundary integral equation of the first kind for Dirichlet boundary value problems in plane elasticity", *Comput. Mech.* **41** (2008), 817–826.

Y. Z. CHEN: chens@ujs.edu.cn
Division of Engineering Mechanics, Jiangsu University, Xue Fu Road 301, Jiangsu 212013, China

X. Y. LIN: xiaoyun39527@yahoo.com
Division of Engineering Mechanics, Jiangsu University, Xue Fu Road 301, Jiangsu 212013, China

Z. X. WANG: wzx-5566@163.com
Division of Engineering Mechanics, Jiangsu University, Xue Fu Road 301, Jiangsu 212013, China

JOURNAL OF MECHANICS OF MATERIALS AND STRUCTURES

Journal of Mechanics of Materials and Structures